Electronic Supplementary Material (ESI) for Physical Chemistry Chemical Physics.

Supplementary Information

Silver oxide model surface improves computational simulation of surface-enhanced Raman spectroscopy on silver nanoparticles

Scott G. Harroun,*[a] Yaoting Zhang,[b] Tzu-Heng Chen,[c,d]
Huan-Tsung Chang,*[c] and Alexis Vallée-Bélisle*[ae]

a. *Laboratory of Biosensors & Nanomachines, Département de chimie, Université de Montréal, Montréal, QC, H3C 3J7, Canada*

b. *Department of Chemistry, Queen's University, Kingston, ON, K7L 3N6, Canada*

c. *Department of Chemistry, National Taiwan University, Taipei, 10617, Taiwan*

d. *Laboratory of Nanoscale Biology, Institute of Bioengineering, School of Engineering, École Polytechnique Fédérale de Lausanne (EPFL), 1015 Lausanne, Switzerland*

e. *Département de biochimie et médicine moléculaire, Université de Montréal, Montréal, QC, H3C 3J7, Canada*

MATERIALS AND METHODS

Chemical Reagents and Instrumentation. 2,6-Diaminopurine (98%), silver nitrate (99.8%), sodium citrate tribasic dihydrate (99.5%) (Sigma-Aldrich, St. Louis, MO, USA) and potassium chloride (Janssen, Beerse, Belgium) were used in this study. All solutions were prepared in ultrapure water from a Milli-Q system (EMD Millipore, Billerica, MA, USA) with 18.2 MΩ·cm resistivity. Raman spectra were recorded with a Nicolet Almega XR Dispersive Raman spectrometer (Thermo Fisher Scientific, Waltham, MA, USA). Spectra were recorded for 30 s with a 780 nm laser at 100% power. The ultraviolet–visible (UV–Vis) spectrum of the Ag NPs was recorded with an Evolution 220 UV–Visible Spectrophotometer (Thermo Fisher Scientific) with a quartz cuvette containing 3 µL of concentrated colloidal Ag NPs and 997 µL ultrapure water. The scanning electron microscopy (SEM) photomicrograph of the Ag NPs was recorded with a S-4800 Field Emission Scanning Electron Microscope (Hitachi, Tokyo, Japan). X-ray photoelectron spectroscopy (XPS) data were obtained using a PHI 5000 VersaProbe instrument (ULVAC-PHI, Kanagawa, Japan). The C1s peak from adventitious carbon-based contamination was used as the reference for calibration of the binding energy. Resultant data were deconvoluted with XPSPEAK41 software. OriginPro 9.0 software (OriginLab Corporation, Northampton, MA, USA) was used for all other data analysis and plotting.

Preparation of Silver Nanoparticles. Ag NPs were prepared based on the popular Lee-Meisel method.[64] In a beaker of 500 mL of vigorously boiling ultrapure water, 0.09 g $AgNO_3$ and 10 mL of 1% w/w trisodium citrate were added, covered, and kept in the dark under magnetic stirring. After 30 min, the Ag NPs suspension was adjusted to 400 mL (due to evaporation) and left to cool to room temperature. The Ag NPs were then concentrated by centrifugation (10x, 1.0 mL aliquots). Next, three 5 µL layers of concentrated Ag NPs were deposited onto a disposable TE100 carbon screen-printed electrode (Zensor Research & Development, Taichung, Taiwan), and allowed to dry before the next layer was added. The electrodes were used because we found that during the subsequent KCl cleaning step for citrate removal, the deposited Ag NPs would often detach from a Si wafer or glass slide, but not from the surface of the electrode. To remove citrate, the dried Ag NPs were treated with 50 µL of 0.5 M KCl for 30 min, and then rinsed carefully with ultrapure water. Finally, 10 µL of 1 mM 2,6-DAP solution was deposited onto the Ag NPs and allowed to dry. Our instrument setup did not permit spectroelectrochemical measurements, but this Ag NP-modified electrode can also be used for electrochemical-SERS (EC-SERS).[65]

Computational Details. Simulated Raman spectra were computed using DFT at the B3LYP level with the 6-311+G(2d,p) (C, N, O and H) and LanL2DZ (Ag) basis sets and the Gaussian 09 software package.[66-70] Optimised ground state structures were used to compute the Raman activities (S_i), which were converted to relative Raman intensity (I_i) using the GaussSum analysis tool with the following relation from the basic theory of Raman scattering.[71-73]

$$I_i = \frac{f(v_0 - v_i)^4 S_i}{v_i\left(1 - \exp\left(\frac{-hcv_i}{kT}\right)\right)}$$

In this equation, v_0 is the exciting frequency (cm^{-1}); v_i is the vibrational wavenumber of the normal mode; h, c, and k are the universal constants; and f is a suitably chosen common normalisation factor for all intensities. None of the simulated spectra had negative frequencies, which confirmed their geometrical optimisation. For the simulated 2,6-DAP spectra, the excitation wavelength was the experimental wavelength (780 nm), temperature was set at 24 °C, and pure Lorentzian band shapes were used with a bandwidth of 10 cm^{-1}. For adenine, melamine and 4,4′-bipyridine, the simulation wavelengths were 532, 633 and 1064 cm^{-1}, respectively. Vibrational modes were assigned by visualisation. All molecular structure images were generated with Avogadro software.[74]

SUPPLEMENTARY DATA

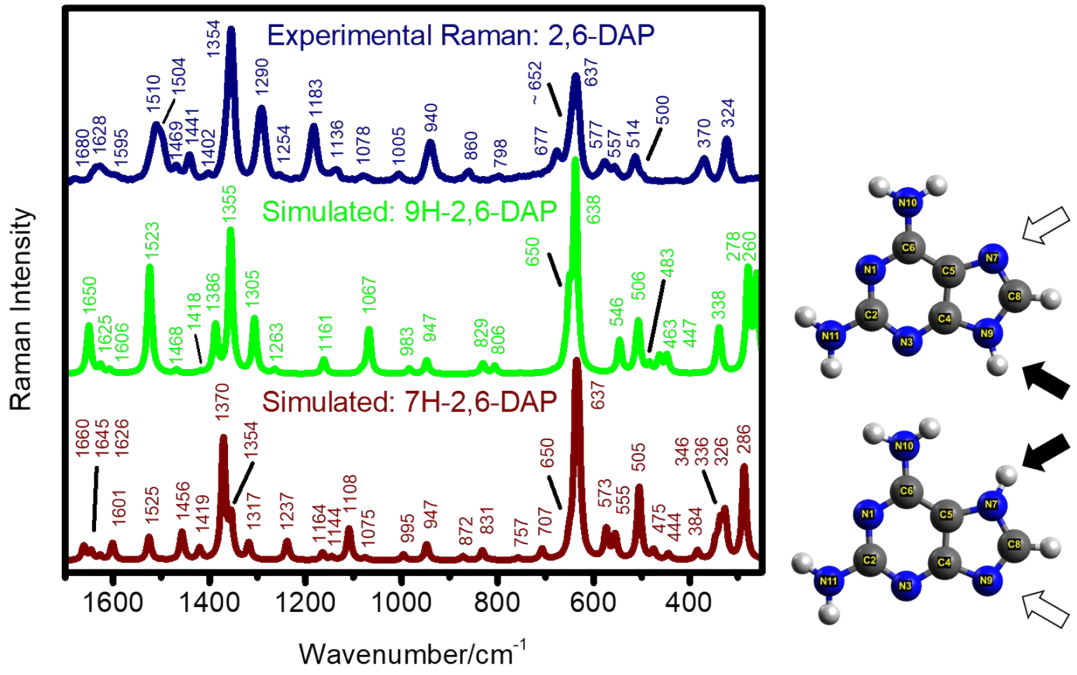

Fig. S1. Raman spectra of 2,6-DAP. The experimental Raman spectrum of 2,6-DAP in the solid phase (powder), consistent with previous reports,[75-77] is shown in comparison with the B3LYP/6-311+G(2d,p) simulated Raman spectra of the 9H-2,6-DAP and 7H-2,6-DAP tautomers.[78] The experimental spectrum is better modelled using the 9H-2,6-DAP tautomer. Shown also are their optimised geometries; see position of the proton on the imidazole ring indicated by the dark arrows. Their computed relative energies are 0.0 and 33.2 kJ/mol, respectively. Atomic colour scheme: blue = nitrogen (N), grey = carbon (C), white = hydrogen (H). See Tables S1 and S2 for vibrational assignments.

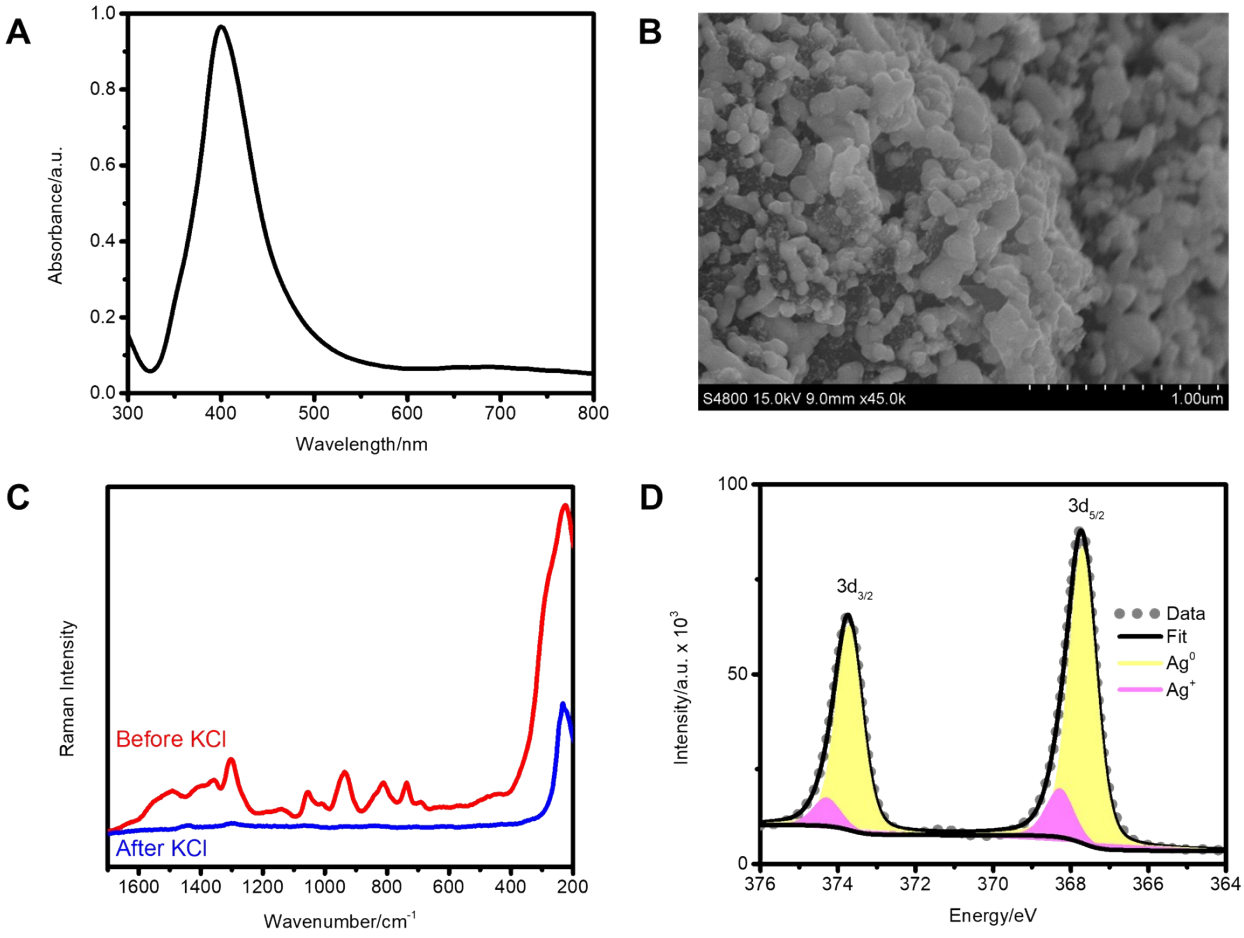

Fig. S2. **Characterisation of Ag NPs.** (A) The UV–Vis spectrum of the colloidal Ag NPs displays a maximum at 400 nm and a full width at half maximum (FWHM) of about 70 nm. (B) Scanning electron microscopy (SEM) of the deposited Ag NPs reveals a mostly spherical shape and diameters of about 50-100 nm. (C) The Raman spectrum of the dried Ag NPs displays the citrate used in their synthesis.[79] Treatment with 0.5 M KCl followed by rinsing with ultrapure water removed it from the spectrum, indicating displacement of the citrate ions. (D) X-ray photoelectron spectroscopy (XPS) of the treated Ag NPs is similar to other SERS-active silver surfaces,[25] wherein the major component is Ag (~85%) along with some Ag^+ (~15%) at the higher binding energy value for the oxidised form.[80] In summary, these are typical Ag NPs akin to those used in many other SERS studies.

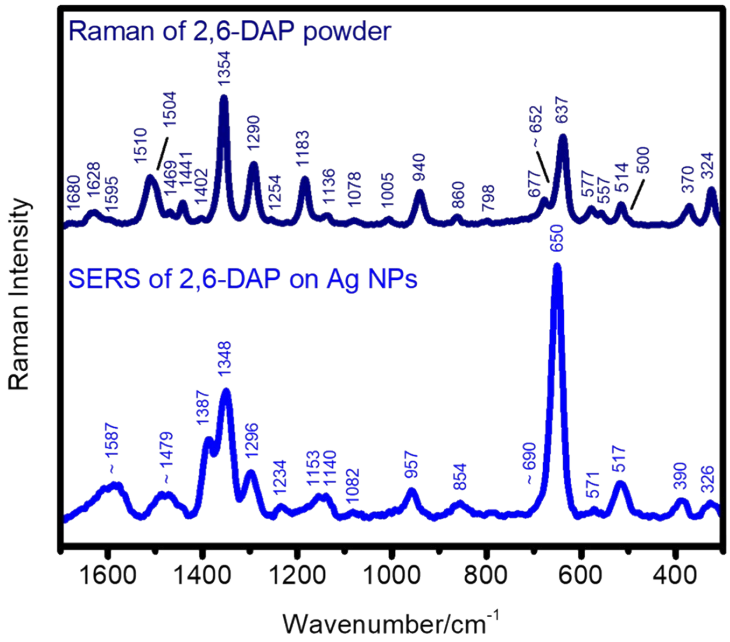

Fig. S3. Comparison of Raman vs SERS of 2,6-DAP. Shown again here for easier comparison are the Raman spectrum of 2,6-DAP powder and the SERS spectrum of 2,6-DAP adsorbed on Ag NPs (see Material and Methods section for more details).

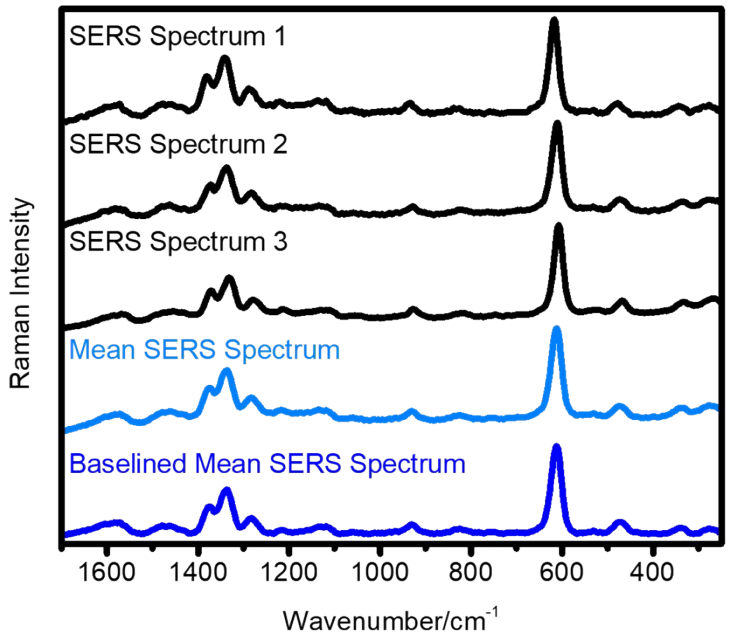

Fig. S4. Mean and baselined SERS spectrum. Three SERS spectra of 2,6-DAP adsorbed on Ag NPs were recorded at different locations on the sample. The mean spectrum was then baselined in OriginPro. For simplicity, it is referred to as the "SERS spectrum" throughout this article.

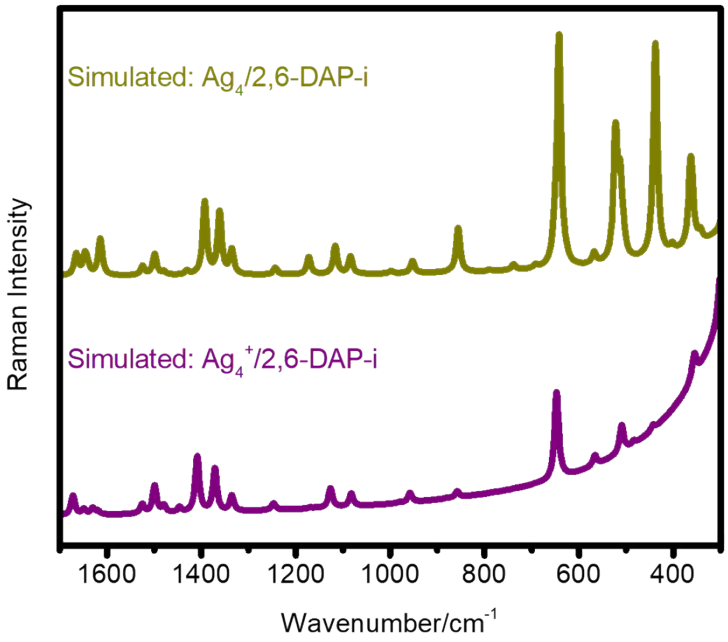

Fig. S5. Removal of background in simulated spectra. Simulated spectra of Ag_4/2,6-DAP-i and Ag_4^+/2,6-DAP-i before baseline correction and normalisation in OriginPro. Ag_4/2,6-DAP-i had a small background and Ag_4^+/2,6-DAP-i had a large background.

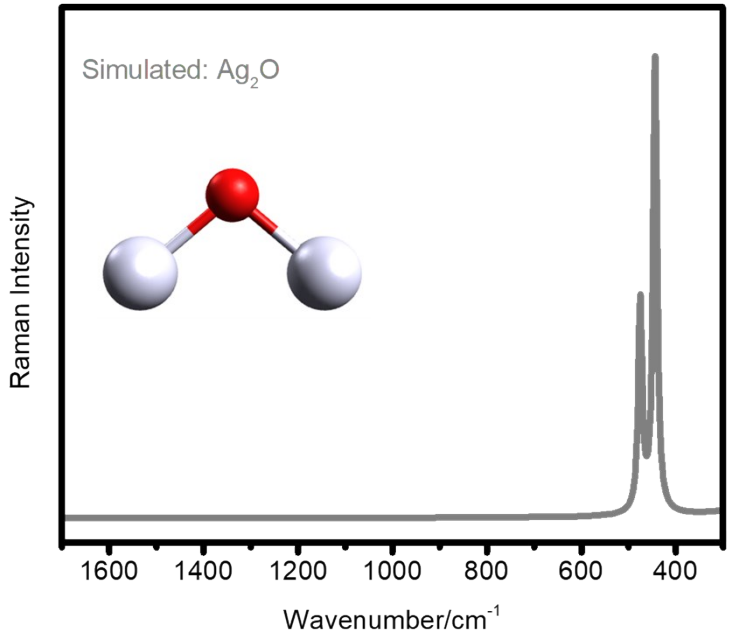

Fig. S6. Control with no ligand on Ag_2O. The optimised structure and simulated Raman spectrum of Ag_2O.

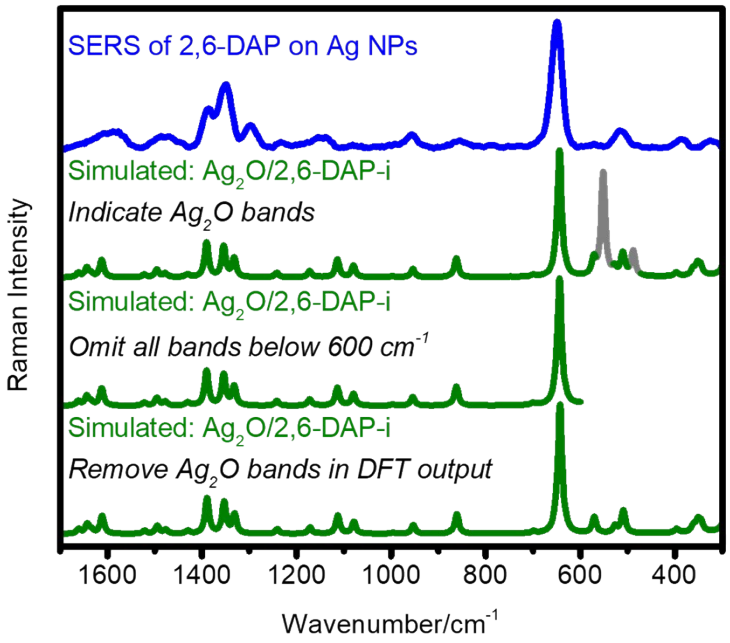

Fig. S7. Presentation of Ag_2O bands. There are different ways to present the simulated SERS spectrum when Ag_2O is employed as the model surface. Recall from our discussion that the two Ag_2O stretching bands in the simulated spectrum will not appear in the experimental spectrum. In Fig. 2, we presented the entire spectrum, but indicated the two Ag_2O stretching bands in a different colour (grey). Alternatively, one could simply not consider all simulated SERS bands below 600 cm^{-1}. This approach is easier and does not require one to check the vibrational origins of the bands, although it could result in other useful bands not being considered. Another option for more experienced computational chemistry researchers would be to manually remove the Ag_2O vibrations (and only these!) from the DFT output file before generating the spectrum. Of course, one must clearly state that the bands have been removed manually. This approach could be employed to create a better visual comparison of the experimental and simulated spectra, although it may not be applicable if Ag_2O vibrations are coupled with other vibrations of the adsorbate.

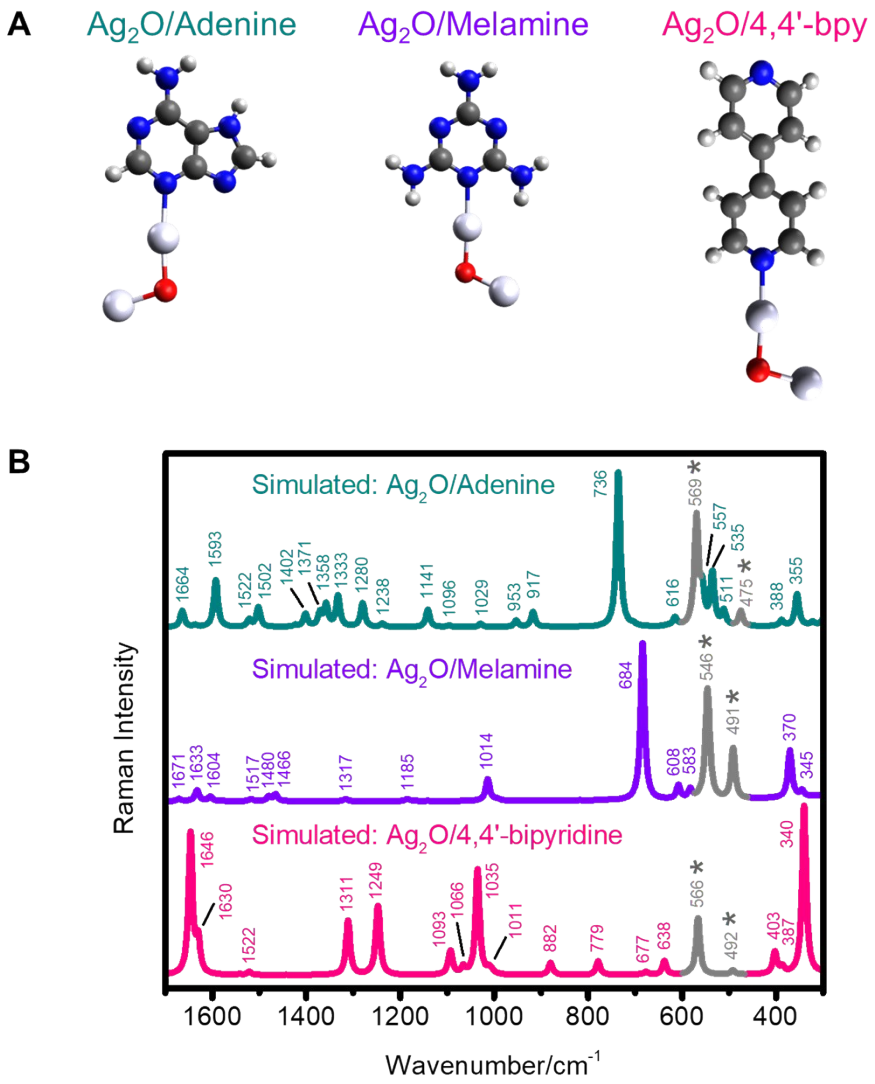

Fig. S8. Simulating the spectra of other molecules. (A) Optimised structures and (B) simulated SERS spectra of Ag_2O/Adenine, Ag_2O/Melamine and Ag_2O/4,4'-bpy. Ag_2O stretching vibrations are indicated with an asterisk (*). Atomic colour scheme: blue = nitrogen (N), grey = carbon (C), red = oxygen (O), white = hydrogen (H), silver = silver (Ag). Laser wavelengths were 532, 633 and 1064 nm, respectively, as used in the cited studies. Ag_2O/Adenine signal intensity was divided by 6 for easier presentation in one figure.

Table S1. Band assignment for 2,6-DAP Raman and SERS spectra. Experimental Raman bands are from 2,6-DAP powder. DFT Raman bands are from the 9H-2,6-DAP tautomer. SERS bands are from 2,6-DAP adsorbed on Ag NPs. DFT SERS bands are from the Ag_2O/2,6-DAP-i complex. Notation for band intensity: very strong (vs), strong (s), medium (m), weak (w) and very weak (vw). Here, the vw designation is used for simulated modes of vibration not seen in the spectrum. Broad bands without a distinct maximum are indicated with (br). Shoulder (sh) bands are also indicated. Bands marked with a question mark (?) indicate uncertain assignment. R5 and R6 indicate modes of vibration for the five- or six-membered rings, respectively. The order of vibrational assignments follows their approximate contribution, as estimated by visualisation.

Raman / cm^{-1}	**DFT Raman / cm^{-1}**	**SERS / cm^{-1}**	**DFT SERS / cm^{-1}**	**Vibrational Assignment**
235 (m)	232 (m)	224 (vs, br)	237 (m)	Ring oop bend, NH_2 wag (N10), NH_2 wag (N11)
-	260 (s)	-	-	NH_2 wag (N10), ring bend
-	-	-	279 (vs)	NH_2 wag (N11)
324 (s)	278 (s)	326 (m)	294 (m)	NH_2 rock (N10), ring bend, NH_2 wag (N11)
-	-	~332 (m, sh)	351 (m)	NH_2 twist (N10), N7–H oop bend, ring oop bend, NH_2 rock (N11)
370 (m)	338 (s)	390 (m)	361 (m, sh)	NH_2 rock (N11), ring bend
-	341 (vw)	-	344 (vw)	Ring oop bend, N9–H oop bend (SERS: N7–H oop bend)
500 (w, sh)	447 (m)	-	-	NH_2 wag (N11)
514 (m)	463 (m)	517 (m)	508 (m)	NH_2 twist (N11)
-	483 (w)	-	396 (w)	N9–H oop bend (SERS: N7–H oop bend), NH_2 twist (N10), ring oop bend
-	-	-	487 (s)	Ag_2O symmetric stretch, some R6 stretch
557 (w)	506 (s)	517 (m)	509 (s)	R6 stretch, some Ag_2O symmetric stretch in SERS
-	512 (vw)	-	-	NH_2 twist (N10), N9–H oop bend, NH_2 twist (N11), R6 stretch
-	-	-	526 (w)	NH_2 wag (N10), ring bend, NH_2 twist (N11)
-	-	-	550 (vs)	Ag_2O asymmetric stretch, some ring bend
577 (m)	546 (m)	571 (w)	570 (m)	Ring bend, some Ag_2O asymmetric stretch in SERS
637 (vs)	638 (vs)	650 (vs)	643 (vs)	Ring bend/stretch (breathing)
652 (m, sh)	650 (s, sh)	-	651 (w, sh)	Ring bend, NH_2 rock (N10), NH_2 rock (N11)
-	659 (vw)	-	630 (vw)	R5 oop bend
677 (m)	683 (vw)	690 (w, sh)	699 (w)	Ring oop bend
-	752 (vw)	-	747 (vw)	Ring oop bend
798 (w)	806 (w)	779 (w)	804 (vw)	C8–H oop bend (less in SERS), ring oop bend
860 (w, ?)	829 (w)	-	873 (vw)	C8–H oop bend, ring oop bend
860 (w, ?)	833 (vw)	854 (w)	861 (s)	Ring stretch
940 (m)	947 (m)	957 (m)	953 (m)	N7=C8–N9 stretch
1005 (w)	983 (w)	-	996 (w)	Ring stretch, NH_2 rock (N10), NH_2 rock (N11)
1078 (w)	1067 (s)	1082 (w)	1078 (m)	Ring stretch, NH_2 rock (N11)
-	1083 (vw)	1140 (w)	1112 (s)	N7–C8 stretch
1136 (w)	1160 (w)	1140 (w) or 1153 (w)	1154 (vw)	R6 bend, ring stretch, NH_2 rock (N10) (SERS: NH_2 rock (N11))
1183 (s)	1161 (m)	1153 (w)	1171 (m)	R6 bend, NH_2 rock (N10), R5 stretch, C2-N11 stretch, (SERS: NH_2 rock (N11))
1254 (w)	1263 (w)	1234 (w)	1240 (m)	C8–H bend, NH_2 rock (N10), N9–H bend (SERS: N7–H bend), ring stretch, NH_2 rock (N11)
1290 (s)	1305 (s)	1296 (m)	1330 (s)	Ring stretch, SERS: No movement for N7–H but has NH_2 rock (N10)
1354 (vs)	1355 (vs)	1348 (s)	1352 (s)	Ring (asym stretch N1–C2 and C4–C5), NH_2 rock (N11), NH_2 rock (N10), N9–H bend (SERS: N7–H

				bend)
1370 (m, sh)	1386 (s)	1387 (s)	1389 (s)	Ring stretch, N9–H bend (SERS: N7–H bend)
1402 (w)	1418 (w)	~1479 (m, br)	1429 (w)	Ring stretch, C4–N9 stretch, C2–N11 stretch, (SERS: C8–N9 stretch, C6–N10 stretch)
1441 (m)	-	~1479 (m, br)	-	Possibly ring stretch (?)
1469 (w)	1468 (w)	~1479 (m, br)	1476 (w)	C2–N3–C4 bend, N7–C8 stretch (SERS: N9–C8 stretch), NH_2 scissor (N11), NH_2 scissor (N10)
1504 (s, sh)	1501 (vw, sh)	~1479 (m, br)	1494 (m)	NH_2 scissor (N10), NH_2 scissor (N11), ring stretch,
1510 (s)	1523 (vs)	~1479 (m, br)	1520 (w)	N7–C8 stretch (SERS: N9–C8 stretch), ring bending, NH_2 scissor (N11), NH_2 scissor (N10)
1595 (w)	1606 (w)	~1587 (m, br)	1610 (s)	NH_2 scissor (N10), R6 stretch, includes NH_2 scissor (N11) in SERS
1628 (m)	1625 (w)	~1587 (m, br)	1633 (w, sh)	NH_2 scissor (N11), NH_2 scissor (N10), R6 stretch
1680 (w)	1650 (s)	~1587 (m, br)	1642 (m)	Ring stretch, N9–H bend, NH_2 rock (N10), NH_2 scissor (N11), SERS: No movement for N7–H.
-	1652 (vw)	-	1660 (w)	NH_2 scissor (N10), NH_2 scissor (N11), R6 stretch
-	3238	-	3239	C8-H stretch
-	3589	-	3559	NH_2 (N11) symmetric stretch
-	3594	-	3567	NH_2 (N10) symmetric stretch
-	3651	-	3656	N9–H stretch (SERS: N7–H stretch)
-	3709	-	3709	NH_2 (N11) asymmetric stretch
-	3719	-	3679	NH_2 (N10) asymmetric stretch

Table S2. DFT simulated Raman bands and corresponding vibrational assignments for the 7H-2,6-DAP tautomer. Notation is the same as in Table S1.

DFT Raman / cm^{-1}	**Vibrational Assignment**
232 (w)	Ring oop bend, NH_2 twist (N10), NH_2 twist (N11)
286 (s)	NH_2 rock (N10), ring bend
326 (s)	N7–H oop bend, ring bend, NH_2 twist (N10)
336 (s, sh)	NH_2 rock (N11), ring bend, N7–H oop bend
346 (m, sh)	NH_2 twist (N10), N7–H oop bend, ring oop bend
384 (w)	NH_2 twist (N10), N7–H oop bend, ring oop bend
444 (w)	NH_2 twist (N11)
475 (w)	NH_2 wag (N11), ring bend
505 (s)	R6 stretch, NH_2 wag (N11)
555 (m)	Ring bend, NH_2 wag (N10), NH_2 twist (N11)
573 (m)	NH_2 wag (N10), ring oop bend
631 (s, sh)	R5 oop bend, R6 stretch
637 (vs)	R5 oop bend, R6 stretch, NH_2 wag (N10)
650 (w, sh)	Ring bend, NH_2 rock (N10), NH_2 rock (N11)
707 (w)	Ring oop bend, NH_2 wag (N10)
757 (w)	Ring oop bend
813 (vw)	Ring oop bend
831 (w)	Ring stretch
872 (w)	C8–H oop bend
947 (m)	N7–C8=N9 bend, R6 stretch
995 (w)	NH_2 rock (N10), C2–N1–C6 stretch, C4–N9 stretch, NH_2 rock (N11)
1075 (w)	C2–N3–C4 bend, C6–N10 stretch, N7–C8 stretch
1108 (m)	N7–C8 stretch, NH_2 rock (N11)
1144 (w)	NH_2 rock (N11), NH_2 rock (N10), R6 bend, R5 stretch
1164 (w)	NH_2 rock (N10), NH_2 rock (N11), ring stretch
1237 (m)	Ring stretch, mostly C5–N7 stretch
1317 (m)	Ring stretch, NH_2 rock (N10), NH_2 rock (N11)
1354 (s)	Ring stretch, C8–H bend, NH_2 rock (N11)
1370 (vs)	Ring stretch, mostly C4–C5 stretch
1419 (w)	N7–C8 stretch, C6–N10 stretch
1456 (m)	C2–N11 stretch, N1–C6 stretch, R5 bend
1497 (vw)	R6 asym stretch, C6–N10 stretch
1525 (m)	C8–N9 stretch, R5 and R6 stretch
1601 (m)	R6 stretch (mostly N1–C2, C4–C5 stretch), NH_2 scissor (N10)

1626 (w)	NH_2 scissor (N11)
1645 (w)	NH_2 scissor (N10)
1660 (m)	Ring stretch (mostly C5-C6 stretch), NH_2 scissor (N10), NH_2 scissor (N11)
3230	C8-H stretch
3552	NH_2 (N10) symmetric stretch
3587	NH_2 (N11) symmetric stretch
3656	N7–H stretch, NH_2 (N10) asymmetric stretch
3659	NH_2 (N10) asymmetric stretch, N7–H stretch
3705	NH_2 (N11) asymmetric stretch

Table S3. Computed relative energies and Boltzmann distribution (*i.e.,* population) for the various Ag^+/2,6-DAP complexes at 298.15 K.

Complex	Relative Energy (kJ/mol)	Population (%)
Ag^+/2,6-DAP-i	0.0	99.99
Ag^+/2,6-DAP-ii	13.1	0.01
Ag^+/2,6-DAP-iii	23.7	0.00
Ag^+/2,6-DAP-iv	24.1	0.00
Ag^+/2,6-DAP-v	36.4	0.00
Ag^+/2,6-DAP-vi	58.5	0.00
Ag^+/2,6-DAP-vii	75.0	0.00

Table S4. Computed Ag–N bond lengths for the various complexes.

Complex	Ag–N bond length (Å)
Ag^+/2,6-DAP-i	Ag–N3 = 2.369 Ag–N9 = 2.478
Ag^+/2,6-DAP-ii	Ag–N7 = 2.310 Ag–N10 = 2.421
Ag^+/2,6-DAP-iii	Ag–N1 = 2.351 Ag–N11 = 2.417
Ag^+/2,6-DAP-iv	Ag–N1 = 2.334 Ag–N10 = 2.500
Ag^+/2,6-DAP-v	Ag–N3 = 2.379 Ag–N11 = 2.395
Ag^+/2,6-DAP-vi	Ag–N1 = 2.380 Ag–N11 = 2.386
Ag^+/2,6-DAP-vii	Ag–N1 = 2.309 Ag–N10 = 2.517
Ag/2,6-DAP-i	Ag–N3 = 2.529
Ag_4^+/2,6-DAP-i	Ag–N3 = 2.218
Ag_4/2,6-DAP-i	Ag–N3 = 2.273
Ag_2O/2,6-DAP-i	Ag–N3 = 2.163
Ag_2O/Adenine	Ag–N = 2.163
Ag_2O/Melamine	Ag–N = 2.163
Ag_2O/4,4'-bpy	Ag–N = 2.158

Table S5. Comparison of methods to simulate SERS of 2,6-diaminopurine on Ag NPs. Here, the wavenumber (cm^{-1}) and relative intensity (%; normalised from 0 to 100 with the most intense band at 650 cm^{-1}) are compared. Wavenumber is shown first, followed by relative intensity in parentheses. Experimental SERS is from this study. For simulated SERS, we compared the Ag^+/2,6-DAP-i, Ag/2,6-DAP-i, Ag_4^+/2,6-DAP-i, Ag_4/2,6-DAP-i, and Ag_2O/2,6-DAP-i complexes. The differences between the experimental and simulated values were used to determine the mean absolute error (MAE) by the formula given below the table.

Experimental	**Ag^+/2,6-DAP-i**	**|Error|**	**Ag/2,6-DAP-i**	**|Error|**	**Ag_4^+/2,6-DAP-i**	**|Error|**	**Ag_4/2,6-DAP-i**	**|Error|**	**Ag_2O/2,6-DAP-i**	**|Error|**
517 (14)*	508 (39)	9 (25)	505 (20)	12 (6)	508 (25)	9 (11)	512 (30)	5 (16)	509 (13)	8 (1)
571 (3)	567 (6)	4 (3)	560 (8)	11 (5)	565 (12)	6 (9)	566 (5)	5 (2)	570 (13)	1 (10)
650 (100)	650 (100)	0 (0)	639 (100)	11 (0)	646 (100)	4 (0)	641 (100)	9 (0)	643 (100)	7 (0)
854 (6)	842 (1)	12 (5)	839 (17)	15 (11)	856 (7)	2 (1)	854 (19)	0 (13)	861 (15)	7 (9)
957 (11)	961 (1)	4 (10)	950 (6)	7 (5)	956 (11)	1 (0)	951 (5)	6 (6)	953 (7)	4 (4)
1082 (2)	1071 (3)	11 (1)	1077 (3)	5 (1)	1081 (15)	1 (13)	1082 (8)	0 (6)	1078 (9)	4 (7)
1234 (4)	1238 (7)	4 (3)	1238 (6)	4 (2)	1245 (8)	11 (4)	1242 (3)	8 (1)	1240 (4)	6 (0)
1296 (18)	1325 (8)	29 (10)	1323 (7)	27 (11)	1334 (19)	38 (1)	1334 (11)	38 (7)	1330 (15)	34 (3)
1348 (50)	1359 (10)	11 (40)	1354 (14)	6 (36)	1370 (52)	22 (2)	1359 (27)	11 (23)	1352 (25)	4 (25)
1387 (31)	1411 (50)	24 (19)	1377 (42)	10 (11)	1407 (67)	20 (36)	1391 (32)	4 (1)	1389 (28)	2 (3)
MAE		**11 (12)**		**11 (9)**		**11 (8)**		**9 (8)**		**8 (6)**

* Format: wavenumber in cm^{-1} (relative intensity in %)

MAE = $\frac{1}{n}\sum_{i=1}^{n} |x_i - y_i|$, where x = SERS wavenumber (or intensity), y = DFT wavenumber (or intensity), n = the number of vibrations.

Note that values are shown here as integers, but no rounding was used in the calculation until the final MAE value.

Table S6. Comparison of methods to simulate SERS of adenine on silver. Here, only wavenumber (cm^{-1}) was compared because we did not have the exact band intensities from other studies. We selected bands that were clearly observed across several studies. Experimental SERS wavenumbers for this comparison were the mean values of seven samples obtained in four studies.[27, 49, 81, 82] For simulated SERS, we compared the Ag_4^+/Adenine complex from the work of Huang *et al.*[27] and our Ag_2O/Adenine complex.

SERS (ref [27])	SERS (ref [49])	SERS (ref [49])	SERS (ref [49])	SERS (ref [81])	SERS (ref [81])	SERS (ref [82])	SERS Mean	Ag_4^+/Adenine (ref [27])	|Error|	Ag_2O/Adenine (This study)	|Error|
624	626	621	624	631	626	619	624	608	16	616	8
732	733	731	732	734	734	730	732	721	11	736	4
958	961	958	954	960	960	958	958	956	2	953	5
1013	1025	1029	999	1026	1026	1030	1021	994	27	1029	8
1113	1137	1117	1094	1136	1135	1119	1122	1106	16	1096	26
1246	1244	1245	1244	1249	1251	1249	1247	1252	5	1238	9
1330	1336	1326	1330	1332	1329	1327	1330	1337	7	1333	3
1401	1397	1399	1397	1397	1398	1396	1398	1391	7	1402	4
1515	1513	1516	n/a	n/a	n/a	1517	1515	1513	2	1522	7
1572	n/a	1568	1586	n/a	n/a	1568	1574	1578	4	1593	19
							MAE		**10**		**9**

Upon comparing the Ag_4^+/Adenine and Ag_2O/Adenine complexes, we see that as determined by the MAE, the latter provides a close but somewhat more accurate simulation of SERS. Notably, the intense ring breathing band, observed experimentally at 732 cm^{-1}, is more accurately simulated by Ag_2O/Adenine. We also noted that Ag_4^+/Adenine has one band at 1363 cm^{-1}, while our Ag_2O/Adenine simulated two bands at 1358 and 1371 cm^{-1}. Experimentally, the 1371 cm^{-1} has been observed, but not the 1358 cm^{-1} band.[49, 81] However, since some bands in this region are somewhat broad in SERS, it remains unclear whether the 1358 cm^{-1} band from Ag_2O/Adenine is simply a bad simulation, or if experimentally it is obscured by one of the more intense and broader bands. Also, Huang *et al.* observed a band at 1650 cm^{-1},[27] which was better simulated by their Ag_4^+/Adenine at 1652 cm^{-1} than by our Ag_2O/Adenine at 1664 cm^{-1}, but this band was not reported in the other studies,[49, 81, 82] so we omitted it from the comparison. In general, the bands above 1500 cm^{-1} were too intense with both methods. Note that the intensity of some bands changes for different silver surfaces, such as the band around 1330 cm^{-1}.[49] Note also that the choice of DFT method could affect the results too, which we did not consider.

Table S7. Comparison of methods to simulate SERS of melamine on silver. Here, only wavenumber (cm^{-1}) was compared because we did not have the exact band intensities from other studies. We selected bands that were clearly observed across several studies. Experimental SERS wavenumbers for this comparison were the mean values of three studies.[28, 83, 84] For simulated SERS, we compared the Ag_4/Melamine complex from the work of An *et al.*[28] and our Ag_2O/Melamine complex.

SERS (ref [28])	**SERS (ref [83])**	**SERS (ref [84])**	**SERS (Mean)**	**Ag_4/Melamine (ref [28])**	**|Error|**	**Ag_2O/Melamine (This study)**	**|Error|**
382	387	387	385	373	12	370	15
573	573	575	574	571	3	583	9
684	680	686	683	688	5	684	1
980	976	979	978	1003	25	1014	36
1185	n/a	n/a	1185	1165	20	1185	0
1494	n/a	1497	1496	1489	7	1480	16
1554	n/a	1553	1554	1543	11	1517	37
1610	n/a	1603	1607	1624	17	1604	3
1690	n/a	1692	1691	1669	22	1671	20
			MAE		**14**		**15**

Compared to our Ag_2O/Melamine complex, the Ag_4/Melamine complex provides a slightly better simulation of the wavenumber of the bands in SERS, as determined by the MAE. However, we note that an experimental SERS band[28] at 1349 cm^{-1} was simulated at 1317 cm^{-1} by Ag_2O/Melamine, but not at all by Ag_4/Melamine. On the other hand, Ag_2O/Melamine has an extra band at 1633 cm^{-1} that was not reported experimentally in the three studies considered. We further observed, however, that for relative band intensity, Ag_2O/Melamine is obviously much better than Ag_4/Melamine (see our Fig. S8 *versus* in ref [28] Fig. 2B and Fig. 6). Finally, we note that another study has used Ag/Melamine and Ag^+/Melamine to simulate SERS, but the bands therein were not labelled, so we could not compare the results.[85]

Table S8. Comparison of methods to simulate SERS of 4,4′-bipyridine on silver. Here, only wavenumber (cm^{-1}) was compared because we did not have the exact band intensities from other studies. We selected bands that were clearly observed across several studies. Experimental SERS wavenumbers for this comparison were the mean values of three studies.[26, 86, 87] For simulated SERS, we compared the Ag/4,4′-bpy, Ag_3/4,4′-bpy and Ag_4/4,4′-bpy complexes from the work of Zhuang *et al.*[26] and our Ag_2O/4,4′-bpy complex.

SERS (ref [26])	SERS (ref [86])	SERS (ref [87])	SERS (Mean)	Ag/4,4′-bpy (ref [26])	|Error|	Ag_3/4,4′-bpy (ref [26])	|Error|	Ag_4/4,4′-bpy (ref [26])	|Error|	Ag_2O/4,4′-bpy (This study)	|Error|
768	770	770	769	768	1	770	1	769	0	779	10
874	n/a	n/a	874	887	13	881	7	886	12	882	8
1015	1018	1014	1016	1019	3	1020	4	1021	5	1035	19
1078	1076	n/a	1077	1098	21	1090	13	1098	21	1093	16
1234	1232	1234	1233	1250	17	1240	7	1250	17	1249	16
1293	1294	1296	1294	1316	22	1316	22	1316	22	1311	17
1514	1514	n/a	1514	1543	29	1543	29	1543	29	1522	8
1609	1611	1610	1610	1649	39	1627	17	1650	40	1646	36
			MAE		**18**		**13**		**18**		**16**

Overall, none of the four methods stands out for simulation of SERS of 4,4′-bipyridine on Ag. For wavenumber of the bands, as determined by the MAE, we see here that Ag_3/4,4′-bpy is the most accurate, followed by Ag_2O/4,4′-bpy, while Ag/4,4′-bpy and Ag_4/4,4′-bpy are the least accurate. However, despite the fact that we did not do a quantitative comparison of the relative intensity of the bands, it is obvious that Ag/4,4′-bpy and Ag_4/4,4′-bpy are the most accurate in this regard, while Ag_3/4,4′-bpy and Ag_2O/4,4′-bpy are less accurate (see our Fig. S8 versus in ref [26] Fig. 3). In summary, none of these methods is the clear winner, although all of the simulations are acceptable.

SUPPLEMENTARY REFERENCES

64. P. C. Lee and D. Meisel, *J. Phys. Chem.*, 1982, **86**, 3391-3395.
65. S. G. Harroun, T. J. Abraham, C. Prudhoe, Y. Zhang, P. J. Scammells, C. L. Brosseau, C. C. Pye and R. D. Singer, *Phys. Chem. Chem. Phys.*, 2013, **15**, 19205-19212.
66. W. Kohn and L. J. Sham, *Phys. Rev.*, 1965, **140**, A1133.
67. A. D. Becke, *J. Chem. Phys.*, 1993, **98**, 5648-5652.
68. C. Lee, W. Yang and R. G. Parr, *Phys. Rev. B*, 1988, **37**, 785-789.
69. P. J. Hay and W. R. Wadt, *J. Chem. Phys.*, 1985, **82**, 299-310.
70. M. J. Frisch, G. W. Trucks, H. B. Schlegel, G. E. Scuseria, M. A. Robb, J. R. Cheeseman, G. Scalmani, V. Barone, G. A. Petersson, H. Nakatsuji, X. Li, M. Caricato, A. V. Marenich, J. Bloino, B. G. Janesko, R. Gomperts, B. Mennucci, H. P. Hratchian, J. V. Ortiz, A. F. Izmaylov, J. L. Sonnenberg, Williams, F. Ding, F. Lipparini, F. Egidi, J. Goings, B. Peng, A. Petrone, T. Henderson, D. Ranasinghe, V. G. Zakrzewski, J. Gao, N. Rega, G. Zheng, W. Liang, M. Hada, M. Ehara, K. Toyota, R. Fukuda, J. Hasegawa, M. Ishida, T. Nakajima, Y. Honda, O. Kitao, H. Nakai, T. Vreven, K. Throssell, J. A. Montgomery Jr., J. E. Peralta, F. Ogliaro, M. J. Bearpark, J. J. Heyd, E. N. Brothers, K. N. Kudin, V. N. Staroverov, T. A. Keith, R. Kobayashi, J. Normand, K. Raghavachari, A. P. Rendell, J. C. Burant, S. S. Iyengar, J. Tomasi, M. Cossi, J. M. Millam, M. Klene, C. Adamo, R. Cammi, J. W. Ochterski, R. L. Martin, K. Morokuma, O. Farkas, J. B. Foresman and D. J. Fox, *Gaussian 09 Rev. A.1*, 2009.
71. N. M. O'Boyle, A. L. Tenderholt and K. M. Langner, *J. Comput. Chem.*, 2008, **29**, 839-845.
72. P. L. Polavarapu, *J. Phys. Chem.*, 1990, **94**, 8106-8112.
73. G. Keresztury, S. Holly, G. Besenyei, J. Varga, A. Wang and J. R. Durig, *Spectrochim. Acta A*, 1993, **49**, 2007-2026.
74. M. D. Hanwell, D. E. Curtis, D. C. Lonie, T. Vandermeersch, E. Zurek and G. R. Hutchison, *J. Cheminform.*, 2012, **4**, 17.
75. J. Florian, P. Mojzes and J. Stepanek, *J. Phys. Chem.*, 1992, **96**, 9278-9282.
76. Z. Dhaouadi, M. Ghomi, P. Mojzes, P. Y. Turpin and L. Chinsky, *Eur. Biophys. J.*, 1994, **23**, 95-104.
77. V. Krishnakumar and R. Ramasamy, *Spectrochim. Acta A*, 2008, **69**, 8-17.
78. Z. Gengeliczki, M. P. Callahan, N. Svadlenak, C. I. Pongor, B. Sztaray, L. Meerts, D. Nachtigallova, P. Hobza, M. Barbatti, H. Lischka and M. S. de Vries, *Phys. Chem. Chem. Phys.*, 2010, **12**, 5375-5388.
79. M. Kerker, O. Siiman, L. A. Bumm and D. S. Wang, *Appl. Opt.*, 1980, **19**, 3253-3255.
80. NIST X-ray Photoelectron Spectroscopy Database, National Institute of Standards and Technology. https://srdata.nist.gov/xps/
81. F. Madzharova, Z. Heiner, M. Gühlke and J. Kneipp, *J. Phys. Chem. C*, 2016, **120**, 15415-15423.
82. X. F. Lang, P. G. Yin, T. T. You, L. Jiang and L. Guo, *ChemPhysChem*, 2011, **12**, 2468-2475.
83. L. Li, S. Yang, J. Duan, L. Huang and G. Xiao, *Spectrochim. Acta A*, 2020, **225**, 117598.
84. N. E. Mircescu, M. Oltean, V. Chiş and N. Leopold, *Vib. Spectrosc.*, 2012, **62**, 165-171.
85. X. Chen, Y. Hu, J. Gao, Y. Zhang and S. Li, *Appl. Spectrosc.*, 2013, **67**, 491-497.
86. A. M. Robinson, L. Zhao, M. Y. S. Alam, P. Bhandari, S. G. Harroun, D. Dendukuri, J. Blackburn and C. L. Brosseau, *Analyst*, 2015, **140**, 779-785.
87. M. Muniz-Miranda, *J. Raman Spectrosc.*, 1996, **27**, 435-437.